LIMNOLOGY
and
OCEANOGRAPHY

ASLO

Limnol. Oceanogr. 9999, 2019, 1–16

doi: 10.1002/lno.11189

Trait-based analysis of subpolar North Atlantic phytoplankton and plastidic ciliate communities using automated flow cytometer

Glaucia Moreira Fragoso [1*,a], **Alex James Poulton** [2,3], **Nicola Jane Pratt** [1], **Geir Johnsen** [4,a], **Duncan Alastair Purdie** [1]

[1]Ocean and Earth Science, University of Southampton, National Oceanography Centre Southampton, Southampton, United Kingdom
[2]The Lyell Centre for Earth and Marine Science and Technology, Heriot-Watt University, Edinburgh, United Kingdom
[3]National Oceanography Centre, Southampton, United Kingdom
[4]University Centre in Svalbard, Longyearbyen, Norway

Abstract

Plankton are an extremely diverse and polyphyletic group, exhibiting a large range in morphological and physiological traits. Here, we apply automated optical techniques, provided by the pulse-shape recording automated flow cytometer—CytoSense—to investigate trait variability of phytoplankton and plastidic ciliates in Arctic and Atlantic waters of the subpolar North Atlantic. We used the bio-optical descriptors derived from the CytoSense (light scattering [forward and sideward] and fluorescence [red, yellow/green and orange from chlorophyll *a*, degraded pigments, and phycobiliproteins, respectively]) and translated them into functional traits to demonstrate ecological trait variability along an environmental gradient. Cell size was the master trait varying in this study, with large photosynthetic microplankton (> 20 μm in cell diameter), including diatoms as single cells and chains, as well as plastidic ciliates found in Arctic waters, while small-sized phytoplankton groups, such as the picoeukaryotes (< 4 μm) and the cyanobacteria *Synechococcus* were dominant in Atlantic waters. Morphological traits, such as chain/colony formation and structural complexity (i.e., cellular processes, setae, and internal vacuoles), appear to favor buoyancy in highly illuminated and stratified Arctic waters. In Atlantic waters, small cell size and spherical cell shape, in addition to photo-physiological traits, such as high internal pigmentation, offer chromatic adaptation for survival in the low nutrient and dynamic mixing waters of the Atlantic Ocean. The use of automated techniques that quantify ecological traits holds exciting new opportunities to unravel linkages between the structure and function of plankton communities and marine ecosystems.

Marine plankton are an extremely diverse and polyphyletic group, revealing a large range in morphological and physiological characteristics, nutritional and light requirements, life-cycle, and predation-avoidance strategies (Falkowski 2004). The overall fitness of individuals within mixed species assemblages is an evolutionary response to the spatial and temporal heterogeneity of pelagic ecosystems, in addition to biotic interactions (e.g., competition, mutualism, and predation) (Litchman et al. 2010). Over global spatial scales, marine plankton communities are biogeographically structured, revealing contrasting patterns of distribution (Follows et al. 2007; Bibby et al. 2009; Cermeño et al. 2010).

Functional traits, which define species in terms of their ecological, physiological, and biogeochemical characteristics, have been shown to be a promising approach to understanding the mechanisms involved in structuring the community as a whole along environmental gradients (McGill et al. 2006). However, this field faces numerous challenges when applied to microscopic organisms, due to the difficulty of quantifying multiple traits at the level of the individual within a diverse community. Intraspecific trait variabilities (e.g., changes in cell organelles, cell size, or colony formation) are also common in marine plankton communities, since their eco-physiological functions may differ depending on environmental variables, such as light levels, nutrient concentrations, and grazing pressures (Litchman et al. 2007, 2010). Automated techniques may fill some of these knowledge gaps by assuring that measurements are observer-independent, in addition to providing data at the individual (or cellular) level that

*Correspondence: glaucia.m.fragoso@ntnu.no

Additional Supporting Information may be found in the online version of this article.

[a]Present address: Centre of Autonomous Marine Operations and Systems, Department of Biology, Norwegian University of Science and Technology, Trondheim, Norway

demonstrate links between community traits and environmental gradients (Pomati et al. 2013).

The automated quantification of multiple traits in a plankton community (e.g., cell size, shape, organelles, cell wall structure, texture, etc.) has been previously performed using several approaches. Examples include imaging flow cytometers, such as the FlowCam imaging cytometer (Sieracki et al. 1998) and the Imaging FlowCytobot (Sosik and Olson 2007). Both instruments use analysis of plankton images, as well as fluorescence properties, to capture plankton variability related to size, morphology, cell-to-cell interactions, and other characteristics (Dashkova et al. 2017). More recently, the combination of fluorescence probes with automated, 3D microscopic imaging (known as environmental High Content Fluorescence Microscopy) allowed not only plankton identification but also computerized quantification of internal cell structures (Colin et al. 2017). These characteristics include DNA content, intracellular membranes, organelles (e.g., chloroplasts, food vacuoles), and cell wall structures (polysaccharides, biogenic silica, calcium carbonate), in addition to biological interactions (e.g., mixotrophy, symbiosis, and parasitism) (Colin et al. 2017). These techniques generate a large amount of data that, if aligned with supervised machine learning algorithms, could tackle the diversity of traits in biological communities across a broad spectrum of spatiotemporal scales (Pomati et al. 2013; Breton et al. 2017; Colin et al. 2017).

The CytoSense instrument (CytoBuoy, b.v., NL), similar to other analytical flow cytometers, provides a non-taxonomical analysis that discriminates particles in aquatic samples, allowing classification of phytoplankton groups based on their individual optical fingerprints (fluorescence emission and light-scattering properties) (Malkassian et al. 2011). A further advantage of this instrument is its capacity to record the "pulse shape" (e.g., Fig. 1), which is an optical fingerprint scan across each particle that provides information about the particle structure (including cellular or subcellular organization) and allows microbial classification (Dubelaar et al. 2004). Moreover, the CytoSense can identify a broader range of particle sizes (from < 1 μm to 1.5 mm in diameter and up to 4 mm in length) that would not be possible with a conventional flow cytometer. The CytoSense also provides images of a selection of those particles (> 10 μm, Fontana et al. 2014), which is useful for species identification of specific plankton groups. The instrument generates a large and complex data set, where many descriptors can provide meaningful eco-physiological information to be used in trait-based analyses, such as cell size, shape, multicellular organization (chain, colony of single cells), and pigment variability (chlorophyll *a*, phycobiliproteins, and degraded chlorophyll compounds) (McFarland et al. 2015).

Here, we apply an automated technique using the CytoSense to analyze trait variability along a longitudinal transect (55–10°W) in the subpolar North Atlantic (Fig. 2). The goals of this article are to: (1) characterize plankton communities (phytoplankton and plastidic ciliates, herein referred to as those able to emit autofluorescence) along gradients of contrasting hydrography comprising Arctic and Atlantic water masses in the sub-Arctic North Atlantic; (2) use the CytoSense descriptors

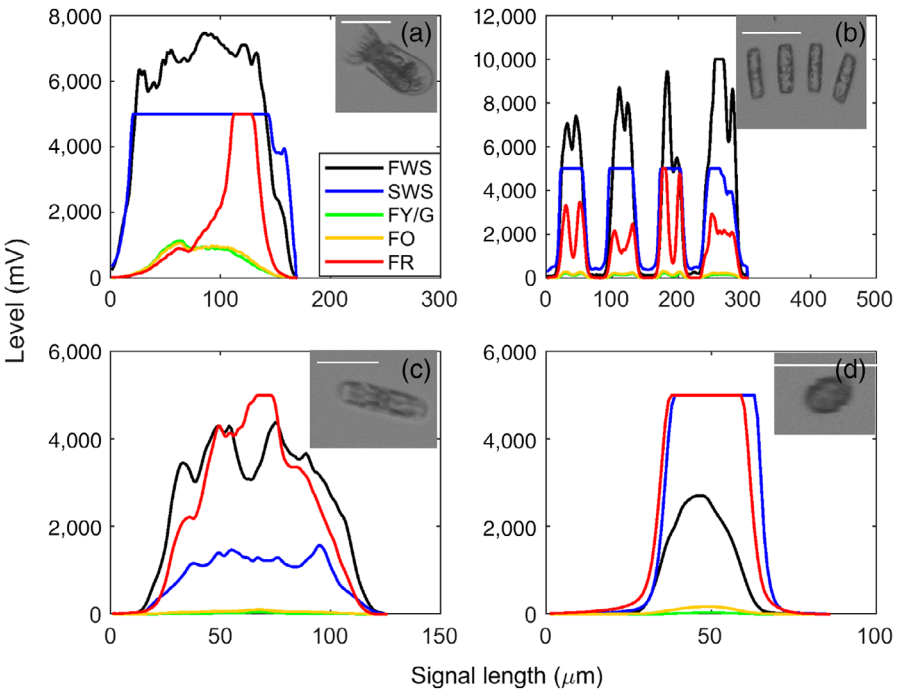

Fig. 1. Example showing the pulse shape and photographic image of: (**a**) plastidic lorica-bearing ciliate (tintinnid), (**b**) *Thalassiosira* sp. chain (diatom), (**c**) *Ephemera* sp. (diatom), and (**d**) thecate dinoflagellate. Colors in the pulse shape refer to the following signals: Forward (FWS, black) and sideward light scatter (SWS, blue), yellow/green (FY/G, green), orange (FO, orange), and red (FR, red) fluorescence. Scale bars are approximately 80 μm in (**a**–**c**) and 60 μm in (**d**).

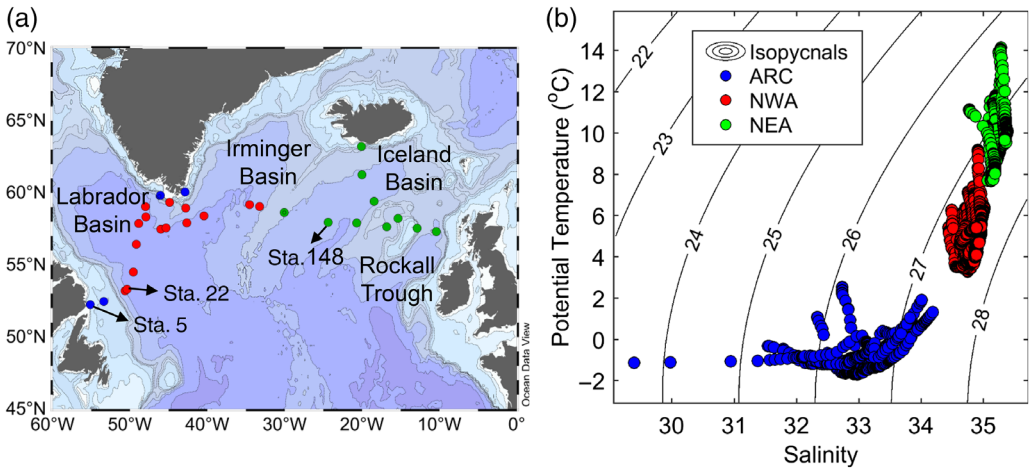

Fig. 2. Biogeographical zones of the North Atlantic showing (**a**) spatial distribution of stations and (**b**) their respective potential temperature and salinity vertical profiles (upper 200 m) with isopycnal contours. Colors are categorized as belonging to the following regions: Arctic (ARC, blue), Northwest (NWA, red), and Northeast (NEA, green) Atlantic.

as examples of plankton functional traits; and (3) investigate the relationship between functional traits and environmental variables among these communities.

Methods

Sample location and collection

Data for this study were collected on board the *RRS James Clark Ross* during the JR302 research cruise, starting on 06 June 2014 on the western side of the Labrador Sea (Canada) and finishing on 21 July 2014, off the west coast of Scotland. Stations were sampled on a west–east transect crossing the shelves and deep ocean basin of the subpolar North Atlantic Ocean, including the Labrador, Greenland, and Irminger Seas (Fig. 2).

Vertical continuous profiles of temperature and salinity were measured using a Seabird 911+ conductivity-temperature-density (CTD) system equipped with a 24 × 10-liter Niskin bottle rosette sampler. Water samples were collected on the upward CTD casts. A stratification index (SI) was calculated as the difference in potential density (σ_θ) values between 60 and 10 m, divided by the respective difference in depth (50 m), as reported in Fragoso et al. (2016).

Nutrient concentrations and chlorophyll *a*

Discrete water samples were collected for chlorophyll *a* (Chl *a*) analysis from the surface (< 10 m). Samples for nutrient analysis (silicate, phosphate, and nitrate) were also collected from the surface (< 10 m), and at every 30–40 m from 10 to 200 m, and every 100 m at depths > 200 m. Samples were measured onboard using a seven-channel SEAL AA3 Autoanalyzer (SEAL Analytical, UK) for dissolved inorganic nutrients. Chl *a* was extracted in 90% acetone for approximately 24 h at −20°C and fluorometrically determined using a Trilogy® Laboratory Fluorometer (Turner Designs, CA, U.S.A.) equipped with Welschmeyer (1994) filters and calibrated against a Chl *a* standard (Sigma, UK) as in Poulton et al. (2016).

Nitrate to phosphate ($\Delta NO_3/\Delta PO_4$) and silicate to nitrate ($\Delta Si(OH_4)/\Delta NO_3$) utilization ratios represent the nutrient reduction in the upper water column (upper 200 m) due to phytoplankton consumption from spring to mid-summer. These reductions were calculated as the difference of the integrated surface (< 10 m) to 200 m nutrient concentration (nitrate, phosphate, and silicate) from the time of sampling (spring to mid-summer) and "winter values" prior to the growth (bloom) season (e.g., Fragoso and Smith 2012), which we consider as the highest concentration between 200 and 500 m at each station.

CytoSense analysis

Water samples (0.2 L) from the surface (< 10 m) were collected and fixed with pre-filtered 50% glutaraldehyde (Fisher Scientific U.K.) at a final concentration of 0.25%. After 15–30 min of fixation, samples were stored at −80°C prior to analysis. Although this method has been reported to cause cell losses (20–40%) for some diatom and dinoflagellate species (Vaulot et al. 1989; Lepesteur et al. 1993), the impact of preservatives is species-specific, given that some species are more robust than others (Menden-Deuer et al. 2001). Thus, it is difficult to make a general prediction of potential cell losses for a mixed population. However, such preservation is still recommended for natural samples preserved for a long period (months to few years) (Dubelaar and Gerritzen 2000; Marie et al. 2005). Samples were analyzed within 24 months of collection using a CytoSense benchtop flow cytometer (CytoBuoy, b. v., NL), which allowed particle examination within a size diameter range of < 1 to 1500 μm.

Similar to other flow cytometers, the suspended particles (sample) are injected into a particle-free carrying fluid (sheath). The laminar flow of the moving sheath fluid aligns the cells in single file sample stream that intersects a laser

(488 nm) (Haraguchi et al. 2017). To match the density and refractive index of the sheath fluid as closely as possible to the samples, prior to analysis, the sheath fluid was replaced with a 3% NaCl solution (w/v) made with Milli-Q water and filtered through a 0.2 μm filter. To avoid bacterial growth, which could interfere with our analysis, the biocide ProClin 950 (Sigma-Aldrich) was added to the new sheath fluid at a final concentration of 0.1% (v/v) before being pumped into the CytoSense.

Triplicate samples (pseudo-replicates) were injected into the CytoSense via a volume calibrated sample pump, which enables the user to collect direct particle concentration data without the need for calibration beads. Samples were transferred to a glass beaker and kept in suspension using a magnetic stirrer. Each sample was run until ~ 10,000 particle events were recorded. To read 10,000 particles, the volumes analyzed ranged from 200 μL, where picophytoplankton were abundant, to 5 mL, for samples with low phytoplankton abundances. Particles are triggered when they intersect a flat 488 nm laser excitation beam of 5 μm high and 300 μm wide as they pass through the flow cell (flow rate of 10.26 μL s^{-1}). For each particle detected, the CytoSense acquires data for the following parameters: forward light scatter (FWS, indicating cell or chain/colony size) and sideward light scatter (SWS), with the latter providing information about cellular granularity and surface complexity. In addition to light-scattering properties, the fluorescence signatures resulting from excitation by the blue light (488 nm) were detected as emitted light at several wavelengths; red Chl *a* fluorescence (FR; 650–830 nm, about 95% of Chl *a* fluorescence arises from Photosystem II, Johnsen and Sakshaug 2007), orange fluorescence (FO, emission from phycobiliproteins; 562–650 nm), and yellow/green fluorescence (FY/G, decaying pigments; 515–562 nm, Fontana et al. 2014). A "curvature" channel adds an extra two-dimensional component by capturing the "split" forward scatter signal from a double laser beam with +45° (left) and −45° (right) polarization angles (Thomas et al. 2018). If a particle has a curved or spiral shape (often observed in diatom chains; e.g., *Chaetoceros curvisetus*), the forward scatter polarization ratio is high.

The trigger channel was set to only measure particles for which the emitted total red fluorescence (FR) was greater than 20 mV from each particle. The reason for this protocol is to target photosynthetic plankton with a strong red fluorescence signal derived from Chl *a* (Marrec et al. 2018). This allows the acquisition of some picophytoplankton FR emission, such as cyanobacteria *Synechococcus* cells, but excludes the cyanobacteria *Prochlorococcus* as ~ 80% of their cellular Chl *a* is bonded to the nonfluorescent Photosystem I, giving a low Chl *a* emission (around 5%, Johnsen and Sakshaug 2007) and is not detected at a trigger level of total FR of 20 mV (Marrec et al. 2018). Fluorescence trigger level and photomultiplier detector sensitivities were optimized prior to running the samples in order to capture the full size range of the samples in a single acquisition, while minimizing background scatter detection (see the CytoSense Manual at www.cytobuoy.com).

During data acquisition, the CytoSense constructs a "pulse shape" for each individual particle, based on the distribution of the fluorescence and light scatter signal along its length. This provides a visual representation of the cross section of a planktonic organism and an estimate of cell length (μm) on the longitudinal axis (according to the known laminar flow rate). It also facilitates the identification of phytoplankton cells with additional signatures from intracellular organelles (e.g., chloroplasts) and plastidic ciliates (aloricate and loricate-bearing) with photosynthetic endosymbionts (Fig. 1).

The pulse shapes of light scatter and fluorescence properties were coupled with a built-in miniature image-in-flow camera (PixeLINK PL-B741 1.3 MP, magnification = ×16, pixel size = 4.8 μm) (PixeLINK, Ottawa, Canada) mounted upward in the capillary tube of the CytoSense instrument (resolution in the size range > 5 μm), which facilitated identification and enumeration of plankton cells based on functional traits. Further information about the functionality of the CytoSense can be found in Malkassian et al. (2011).

CytoSense descriptors and functional traits

For each of the six channels (FWS, SWS, FR, FY/G, FO, and curvature), the CytoClus 4 software (CytoBuoy, Nieuwerbrug, The Netherlands; Dubelaar and Gerritzen 2000) calculates several parameters for each particle, including length (μm), integrated total signal (area under the curve), maximum signal amplitude, average signal strength, fill factor (area of each signal compared to background), signal asymmetry, and number of cells (number of peaks in pulse shape). The representation of each parameter and more detailed information can be found in the Supporting Information Fig. S1 and in Fontana et al. (2014).

The parameters used in this article to derive functional traits are listed in Table 1. Cell size is considered a major functional trait in plankton, given that it is correlated with many physiological, ecological, and life history traits (Marañón 2015). In this study, FWS length is used to represent cell/chain size. Curvature length and number of signal peaks per particle represent multicellular organization (chains and/or colonies of single cells). The bio-optical signal peaks represent, approximately, the number of cells in a particle (chain), while the curvature represents how the particles deviate from the center of the flow. Chains of cells with a high curvature value (i.e., with a spiral shape) will by their nature be longer than their FWS length suggests. Therefore, a combination of increased curvature and cell number will indicate the presence of long chains (e.g., diatoms). FWS asymmetry provides information about the shape of the particles, whereas the FWS fill factor represents particle shape diversity, where a high value (near 1) represents a particle with a square shape. We, therefore, assumed the opposite (i.e., 1-Fill Factor) to represent a particle with a shape resembling a sphere.

Maximum SWS signal is correlated with the refractive index of the particle and represents high internal/external structure

Table 1. Technical and biological explanation of the assigned traits from the CytoSense output descriptors in this study.

CytoSense descriptor (output as is)	Technical interpretation	Biological interpretation	Trait assigned in this study as
FWS length	Estimation of the actual particle length derived from the FWS signal	Cell/chain/colony size and length	Size
Curvature length	The deviation of the signal from the center of the background box	Indication of how long the cell/chain/colony is. Usually, the more curved the chain/colony, the longer it is.	Chain/colony
FWS number of cells	Approximation, rather than the actual number of cells. The number of meaningful peaks in a signal	Approximated number of cells per chain	Cells per chain
1-FWS fill factor	The fill factor is the ratio of the area under the FWS signal curve and the area under the rectangular bounding box of the signal (background). If the signal resembles a block (it is constant), the fill factor will approach 1. Calculating 1-fill Factor means the opposite—that the signal consists of a narrow peak	Assumes cell morphology, where high values indicate that the cell/chain/colony is spherical and low values mean that it has a square shape	Sphere
FWS asymmetry	Uses the relative location of the Center of the Gravity (where the signal is concentrated) to estimate the asymmetry of a particle	How asymmetric cell/chain/colony is	Asymmetry
(FO total/FR total)/FWS total	The ratio of the area of FO and the area of FR pulse signals per volume (FWS total)	Ratio of the concentrations of pigments that fluoresces in orange (e.g., accessory pigments, including phycoerythrin) to chlorophyll *a* concentrations related to volume	Phycoerythrin/ chlorophyll *a* (PE/Chl *a*)
FR total/FWS total	The ratio of the total FR and total FWS pulse signals	The ratio of chlorophyll *a* to the ratio of volume	Chl *a*/volume (Chl *a*/Vol)
SWS maximum	The highest SWS signal value of a pulse	How light is scattered (refractive index) from the cell/chain/colony due to high internal (vacuoles) and external (e.g., processes) complexity	Structural complexity

Pulse signals used: forward (FWS) and sideward scatter (SWS), red (FR), and orange fluorescence (FO). More details on the descriptor information is in Supporting Information Fig. S1.

complexity, such as cell wall granularity (e.g., coccoliths in coccolithophores), ornaments (processes, setae, and heavily silicified cell walls in diatoms), and internal vacuoles (also commonly found in large diatoms; Woods and Villareal 2008). The FWS total signal has been suggested as a suitable descriptor for particle volume (Haraguchi et al. 2017), thus, photo-physiological information for the community, such as the amount of Chl *a* per cell volume (Chl *a*/Vol), either as a single cell or chain, was analyzed by FR total/FWS total. Other fluorescence signatures, such as FO total/FR total related to their size (FWS total), provide information about the pigment composition in the phytoplankton community, allowing the differentiation of cyanobacteria from other picophytoplankton groups, given that they contain high concentrations of phycobiliproteins (e.g., phycoerythrin [PE]), which fluoresce in the orange part of the spectrum, per cell size (FWS total) (Table 1).

Plankton group discrimination

To allow a proper interpretation of trait variability among functional groups, photosynthetic plankton were classified and counted using the CytoClus 4 software. The groups were classified a posteriori. A manual clustering of the data was primarily selected based on FWS length (μm) vs. FO total, since size and pigments (Chl *a* and PE) were the main notable traits observed within groups (see manual gating information in the Supporting Information Fig. S2). However, cytograms of a variety of other parameters (e.g., FWS length [μm] vs. FR total; see

previous section) were performed to confirm the identity of the phytoplankton groups (Supporting Information Fig. S3). The manual clustering consists of selecting points in the scatterplot, which represents the populations of cells with common characteristics (termed "gating" in flow cytometry) that were assigned to specific plankton groups based on their respective properties of light scatter and autofluorescence. Example of cytograms showing the assignment of different plankton groups as a function of their bio-optical properties are shown in Fig. 3.

A total of nine groups were manually classified based on size (microplankton, nanoplankton, and picoplankton and FO signal (Fig. 3, see also manual gating in Supporting Information Fig. S2). The gating structure was kept the same for all samples analyzed to consistently categorize the distinct groups. Microplankton were classified as: (1) Micro-HighFO, including some plastidic (autofluorescent) ciliates as confirmed by images and pulse-shape; (2) Micro-HighFWS, including large, chain-forming diatoms, also confirmed by images and pulse-shapes; (3) Micro-MediumFWS, consisting of diatoms (confirmed by images) with medium FWS emission (see below); and (4) Micro-LowFO, including some diatoms (as confirmed by images as well) with low FO emission (see below). Similar to microplankton, nanophytoplankton were classified regarding size (4–20 μm) and FO signal as: (5) Nano-HighFO, which consisted possibly of PE-containing cells, including cryptophytes and some dinoflagellates; (6) Nano-MediumFO; and (7) Nano-LowFO, likely non-PE containing cells. Picophytoplankton were classified as: (8) Pico-HighFO, possibly consisting of PE-containing prokaryotes, such as *Synechococcus*-like cells; and (9) Pico-LowFO, such as non PE-containing picoeukaryotes.

Micro-HighFO, which included plastidic ciliates, were identified based on their large size (> 20 μm), presence of FR emission (*see* Supporting Information Fig. S3a), and high FO emission characteristics (Fig. 3a). The term "plastidic" for ciliates in this study is for simplification, since autofluorescence is possibly due to endosymbiosis of a whole photosynthetic cell (Qiu et al. 2016) or acquisition of chloroplasts containing Chl *a* and orange fluorescent PE from cryptophytes, such as observed in the ciliate *Mesodinium rubrum* (Gustafson et al. 2000) and in the marine oligotrich *Strombidium rassoulzadegani* (Schoener and McManus 2012). High FY/G signal in plastidic ciliates has also been observed in this (Fig. 1a; *see* Supporting Information Fig. S3m,o) and other studies (Dubelaar et al. 2004).

Micro-HighFWS, which included diatom chains, were classified based on high FWS signal and FO signal (Fig. 3a–c) as well as FR signal (Bonato et al. 2015; Supporting Information Fig. S3a). In general, FWS total and FR total correlated positively (average signal of all sites: FR total = 1.15 FWS total$^{0.91}$, r^2 = 0.83), meaning that the larger the particle, the stronger the

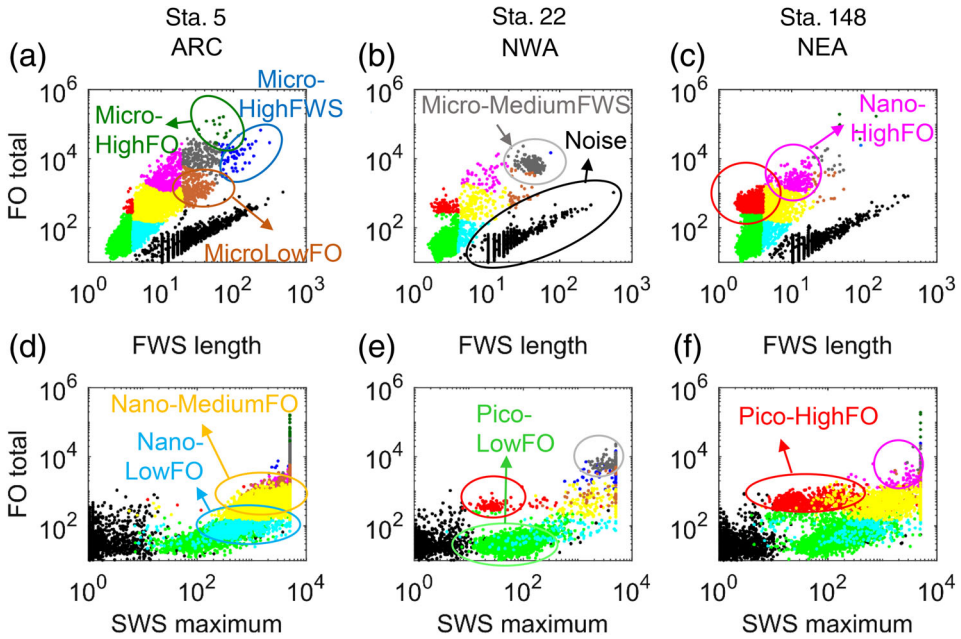

Fig. 3. Cytograms for samples from stations represented in Fig. 2 that belongs to the distinct hydrographical regions of the subpolar North Atlantic: Arctic (ARC, Sta. 5, left), Northwest Atlantic (NWA, Sta. 22, middle), and Northeast Atlantic (NEA, Sta. 148, right) based on: (**a**–**c**) orange fluorescence (FO) total and forward scatter (FWS) length and (**d**–**f**) FO total and sideward scatter (SWS) maximum. Plankton groups are represented in different colors: Pico-LowFO (likely picoeukaryote, light green), PE-containing nanophytoplankton (defined as Nano-HighFO, pink) and non-PE containing nanophytoplankton (defined as Nano-MediumFO, yellow, and Nano-LowFO, cyan), Pico-HighFO (*Synechococcus*-like cells, red), Micro-HighFO (identified as plastidic ciliates in some images, dark green), Micro-LowFO (which includes small diatoms, brown), Micro-MediumFWS (including medium diatoms, gray) and Micro-HighFWS (mostly large, chain-forming diatoms, dark blue), in addition to noise (black). Additional cytograms are shown in Supporting Information Fig. S3.

FR autofluorescence (from Chl *a*) observed. High FR total signal also correlated positively with FO total signal (FR total = 27.16 FO total$^{0.91}$, r^2 = 0.85), since the higher the FR signal from chloroplasts, the higher the spillover of FO signal, due to the overlap between these two channels. Thus, to determine whether FO originated from PE or was an artifact of strong FR signal, the relationship of FO and FWS was examined, where PE-containing cells have a higher FO/FWS than non-PE containing ones (Fig. 3a–c). Diatoms were separated into different size ranges (FWS length) and consequently FO (Fig. 3a–c) as well as FR signal ranges (Supporting Information Fig. S3a–c): Micro-HighFWS, often found as large diatom chains (FWS length; mean [μ] = 145 μm; standard deviation [σ] = 61 μm) (see example in Fig. 1b), Micro-MediumFWS, diatoms found as single cell or medium-sized chains (μ = 37 μm, σ = 9 μm) with moderate FR signals (*see* Supporting Information Fig. S3a–c), which also reflects a moderate FO (Fig. 3a–c), possibly due to Chl *a*, or Micro-LowFO, small diatoms (also single cells or small chains [μ = 25 μm, σ = 3 μm] and lower Chl *a*) (Fig. 3a–c). As a photograph of some large particles (> 10 μm; Fig. 1) is taken simultaneously with each pulse shape, photographs of plastidic ciliates and diatoms were used to confirm the manual gating of these assigned groupings.

Other groups, which were too small to have their identification visually confirmed from the photographs (with the exception of some dinoflagellates; *see* Fig. 1d), were classified based on their optical signature. Pico-HighFO, considered in this study as *Synechococcus*-like cells, were discriminated through their small size (FWS length < 4 μm) and a significant ratio of FO/FR total (mostly > 1; Supporting Information Fig. S3r) due to their high PE content compared to Chl *a* (Thyssen et al. 2014, 2015). PE-containing nanophytoplankton (Nano-HighFO), which includes cryptophytes and some dinoflagellates, were classified and grouped together based on high FO signals, but distinguished from the former group (*Synechococcus*-like) by their larger cell size (FWS from 4 to 20 μm) (Fig. 3). High FO in PE-containing nanophytoplankton occurs either due to presence of PE (in the case of cryptophytes) (Thoisen et al. 2017) or due to the ingestion of small photosynthetic plankton (in the case of dinoflagellates).

Another two groups consisted predominantly of non PE-containing nanophytoplankton (Nano-MediumFO and Nano-LowFO), which likely includes mixed and unresolved nanophytoplankton groups such as coccolithophores, non-calcifying haptophytes, dinoflagellates, and nano-sized diatoms (4 - 20 μm). This group was discriminated based on cell size (FWS length signal from 4 to 20 μm), moderate FO signal and high SWS maximum caused by the sideward light scatter of inorganic cell components, such as coccoliths, cellulose plates, and opal frustules. Coccolithophores have been resolved previously using the CytoSense (e.g., Bonato et al. 2015, 2016), however, in our study, we could not confidently separate coccolithophores from other small taxa due to similarity in the CytoSense signal from cells with calcium carbonate coccoliths and cellulose plates. Other non PE-containing flagellates were classified based on their cell size (Nano-LowFO, FWS length signal from 4 to 12 μm and Pico-LowFO, FWS < 4 μm) and low FO and FR signals (Fig. 3a-c; Supporting Information Fig. S3a–c). Data that did not represent plankton cells (referred to as noise) were identified observing the pulse shape feature of the particle (*see* Supporting Information Fig. S4). Data classified as noise were manually grouped and removed from further analyses.

The FWS total signal has been suggested as a better descriptor for particle (cells and colonies/chains) volume than SWS (Haraguchi et al. 2017), so in this study, volume (Vol) is taken as FWS total. To estimate plankton group biovolume, Vol was converted to μm^3 following Haraguchi et al. (2017), where biovolume (μm^3) = 4.24×10^{-6} Vol$^{1.88}$. Haraguchi et al. (2017) derived their algorithm from the log–log relationship between the average integrated FWS total signal of a taxon (18 species in total) and the cellular biovolume (μm^3, 20–50 cells per taxon) calculated from separate microscope measurements. Phytoplankton and ciliate biovolumes were standardized among samples to demonstrate the relative biovolume at each site.

Relative biovolume of size-based photosynthetic functional groups (microplankton [including plastidic ciliates], nanoplankton, and picoplankton) were defined as the fractions of the sum of the following groups divided by the total:

Micro - plankton (approx. > 20 μm, M_f) = Micro - HighFO + Micro - MediumFWS + Micro - LowFO + Micro - HighFWS;

Nano - plankton (approx. 4 to 20 μm, N_f) = Nano - HighFO + Nano - MediumFO + Nano - LowFO;

Pico - plankton (approx. < 4 μm, P_f) = Pico - HighFO + Pico - LowFO.

Statistical analyses

Using the CytoClus 4 software, the mean value of each parameter (*see* "CytoSense descriptors and functional traits" section) was calculated from the pooled plankton groups ("all data but noise," see manual clustering in Supporting Information Fig. S2) in each sample and exported as .csv files. Each trait derived from the CytoClus 4 (calculations are explained in Table 1) were normalized among samples, to determine the stations with lowest (value = 0%) or the highest (100%) trait value.

Multivariate analyses were performed on the normalized trait data using PRIMER-E (version 7) software (Clarke and Warwick 2014). Relative biovolume (percentages) of each plankton group among the different stations and among the groups themselves were displayed along the contrasting hydrography using "Shade Plot task" in the PRIMER-E software.

To analyze the overall variance of plankton traits from stations of distinct hydrographical regions, principal component analyses (PCA) were applied to the normalized trait values (after square-root transformation) for each sample using the PRIMER-E software. Pie charts were constructed in the PCA plots using the PRIMER-E software to examine the associations

between plankton size groups (picoplankton, nanoplankton, and microplankton) and community trait parameters.

ANOVA and post hoc Tukey-Kramer tests were used to determine the overall significance difference (set at $p < 0.05$) of environmental factors and traits among samples from distinct oceanographic regions using Minitab Software (Version 18, Minitab, University Park, PA, U.S.A.). Pair-wise Pearson product-moment correlations and statistical significance (at $p < 0.05$) were calculated among traits themselves and between traits and environmental values using the statistical software R (Version 3.3.3) and the *corrplot* package.

Results

Hydrography and nutrient distributions

The subpolar North Atlantic was divided into three distinct zones based on hydrography (Arctic, Northwest Atlantic [NWA], and Northeast Atlantic [NEA]), with temperature, salinity, and nutrient utilization ratios varying in upper (0–200 m) waters (Fig. 2). In general, cold (< 3°C), fresh (salinity < 34.5), and low-density waters (σ_θ < 27.5 kg m^{-3}) were found on the shelves, near Canada (the Labrador Shelf) or on the southern tip of Greenland (Greenland Shelf), indicating the influence of waters originating from the Arctic outflow, herein defined as the ARC region. Waters from ARC were the most strongly stratified in this study (see also Supporting Information Fig. S5a).

The NWA region included the central portion of the Labrador Basin (between Canada and Greenland) and the Irminger Basin (Fig. 2a). The upper 200 m of the NWA had the densest (27–28 kg m^{-3}) water mass observed in this study and, compared to Arctic-related waters, was warmer (2–9°C), more saline (34.3–35.2) and had features of modified Atlantic waters (Fig. 2b). Waters from the NWA were the least stratified in this study (Supporting Information Fig. S5a).

The third water mass belonged to the NEA region, which comprised the waters from the Iceland Basin and Rockall Trough near Scotland (Fig. 2a). The water mass from NEA was characterized as the most saline (> 34.8) and warmest (> 8°C), with moderate stratification and density values (27.5–26.5 kg m^{-3}) compared to the other water masses (Fig. 2b; Supporting Information Fig. S5a). The temperature and salinity (T–S) properties from the upper 200 m were not only related to the spatial distribution of these stations (Fig. 2), but also to the temporal time-frame at the interval of sampling, as waters from the Labrador Shelf (near Canada) were sampled earlier in the season (mid-June) while samples from the NEA were collected in mid-July.

Plankton distribution

Microplankton, including the groups Micro-LowFO (consisted of small single-celled diatoms), Micro-MediumFWS (*Ephemera* spp. [*see* Fig. 1c] and short diatom chains), Micro-HighFWS (large diatom chains; Fig. 1b), and Micro-HighFO (plastidic ciliates, aloricate, and loricate-bearing; Fig. 1a), were more abundant in terms of both concentration (counts L^{-1}) and relative biovolume in the ARC region, being rarely observed in the NEA (Fig. 4). In contrast, Pico-LowFO (likely picoeukaryote cells) had the highest concentration (counts L^{-1}) and relative biovolume in Atlantic waters (NWA and NEA). Nano-MediumFO (non PE-containing nanophytoplankton), such as coccolithophores, small dinoflagellates, or diatoms (4 - 20 μm), had higher concentrations (counts L^{-1}) and relative biovolume in ARC and NEA waters. Nano-HighFO (PE-containing nanophytoplankton), including cryptophytes and some dinoflagellates, in addition to Nano-LowFO (non PE-containing nanophytoplankton), were all found in similar concentrations (counts L^{-1} and relative biovolume) throughout the regions of the sub-Arctic North Atlantic (Fig. 4). Pico-HighFO (*Synechococcus*-like cells) were observed in higher concentrations in Atlantic waters, particularly in the NEA (Fig. 4).

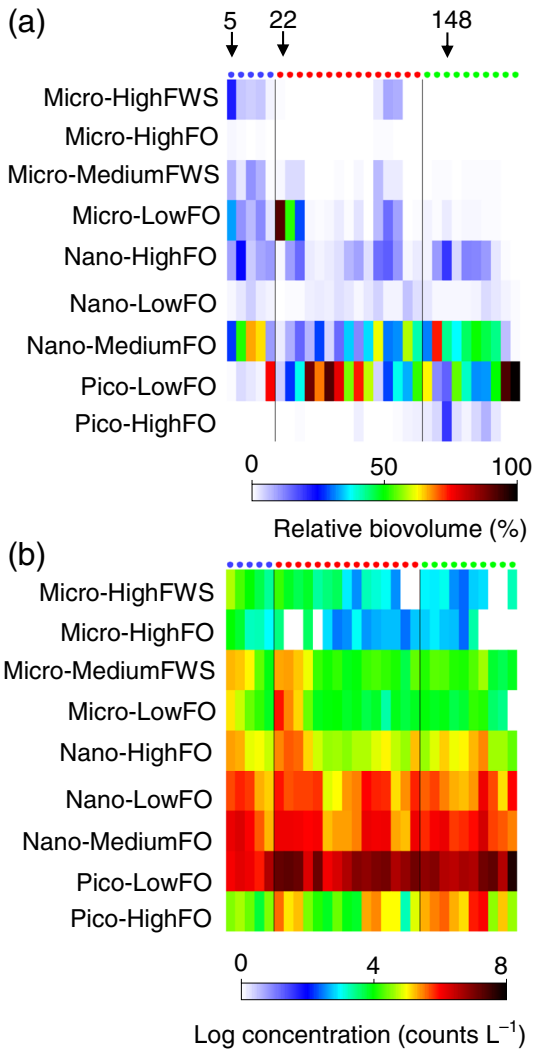

Fig. 4. Shade plot showing the (**a**) relative biovolume (percentage) and (**b**) concentration (log-transformed counts L^{-1}) of plankton groups at each site belonging to the distinct hydrographical regions of the subpolar North Atlantic: Arctic (ARC, blue), Northwest (NWA, red) and Northeast (NEA, green). Arrows refer to station name, where cytograms were plotted as in Fig. 3.

Traits, plankton groups, and size variability

Plankton groups from distinct hydrographical regions of the sub-Arctic North Atlantic showed distinct functional traits, which explained 64.1% of the compositional variability among regions on the first PCA axis (PC1) and a cumulative proportion of 97.7% of variability across four PCA axis (Table 2; Fig. 5). Compared to the other hydrographic regions, plankton groups from Arctic waters (ARC) were larger, more asymmetric and had higher external (setae, cell processes) or internal structural complexity (vacuoles), as well as being colonial (or chain) with a greater number of cells per chain (Fig. 5a). Plankton groups in the ARC also consisted of a greater proportion of microplankton (plastidic ciliates and diatoms) (Fig. 5b).

Conversely, functional traits of plankton in Atlantic waters were significantly different from the Arctic (ARC) (one-way ANOVA, $p < 0.05$; see also Supporting Information Fig. S6). Traits of plankton from the Atlantic were: small cell size (most cells were < 4 μm), spherical shape, solitary form, with high PE/Chl *a* and Chl *a*/Vol (Fig. 5a). Between regions of the Atlantic (NWA and NEA), most functional traits were not significantly different (one-way ANOVA, $p < 0.05$), except for shape, which was dominated by more spherical forms in the NEA compared with the NWA region (one-way ANOVA and post hoc Tukey-Kramer tests, $p < 0.05$; see also Supporting Information Fig. S6d). Atlantic waters had higher contributions of picophytoplankton (*Synechococcus*-like and picoeukaryotes) and lower contributions of microplankton (diatoms and plastidic ciliates) than Arctic waters, whereas nanophytoplankton contribution (PE and non PE-containing nanophytoplankton) varied in Atlantic waters (Fig. 5b).

Traits and environmental relationships

Pairwise comparisons showed that some traits presented positive or negative correlations among themselves, or when related to environmental variables (Pearson product-moment correlations; Fig. 6). Large, colonial and asymmetric phytoplankton, with greater extracellular (setae or processes) and/or internal cellular complexity (internal plastids and vacuoles) were positively correlated with colder, fresher, and strongly stratified waters ($p < 0.05$), with higher $\Delta Si(OH)_4/\Delta NO_3$ utilization ratios. Conversely, small, spherical, single cells with high PE/Chl *a* were positively correlated with warm and more saline waters, with higher $\Delta NO_3/\Delta PO_4$ utilization ratios, whereas Chl *a*/Vol correlated negatively with temperature ($p < 0.05$, Fig. 6).

Table 2. List of factor loadings of principal component analysis on traits used in this study.

Axis	1	2	3	4
Eigenvalues	26.9	9.25	3.62	1.21
Proportion of variance (%)	64.1	22.1	8.6	2.9
Cumulative proportion (%)	64.1	86.1	94.8	97.7
Variables				
Asymmetry	−0.267	0.607	−0.663	0.301
Cells per chain	−0.255	−0.374	−0.142	−0.164
Size	−0.407	0.008	0.187	0.152
Chain/colony	−0.404	−0.086	−0.012	−0.381
Structural complexity	−0.451	−0.048	−0.028	−0.073
Sphere	0.116	−0.62	−0.672	0.051
PE/Chl *a*	0.372	0.305	−0.229	−0.728
Chl *a*/Vol	0.424	−0.067	0.021	0.42

Abbreviations refer to phycoerythrin to chlorophyll a (PE/Chl *a*) and Chl *a* to volume (Chl *a*/Vol) ratios.

Discussion

Patterns of plankton community structure

The subpolar North Atlantic presents a complex hydrographic environment, where waters of Arctic and Atlantic origin divide the region into different zones with defined biogeographical provinces (Longhurst et al. 1995; Head et al. 2003; Fragoso et al. 2016). In this study, the distinct water masses of the sub-Arctic North Atlantic showed dissimilar plankton functional groups. In waters of Arctic origin (ARC), a greater proportion of large (> 20 μm) microplankton were observed, including diatoms as

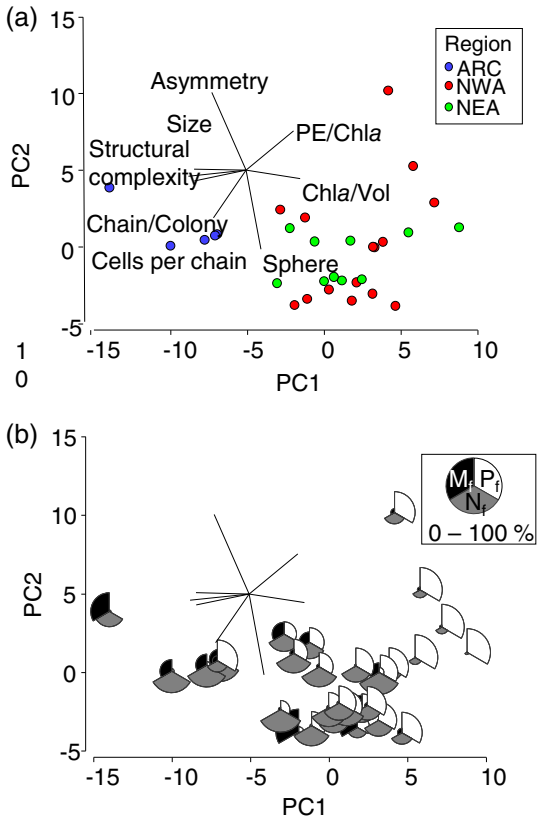

Fig. 5. Principal components (PC) analysis of trait variables as a function of (**a**) stations from different regions (Arctic: ARC, blue; Northwest: NWA, red; Northeast Atlantic: NEA, green) and (**b**) relative biovolume of size classes: photosynthetic picoplankton (P_f, white), nanoplankton (N_f, gray), and microplankton and plastidic ciliates (M_f, black). Abbreviations refer to phycoerythrin to chlorophyll *a* (PE/Chl *a*) and Chl *a* to volume (Chl *a*/Vol) ratios.

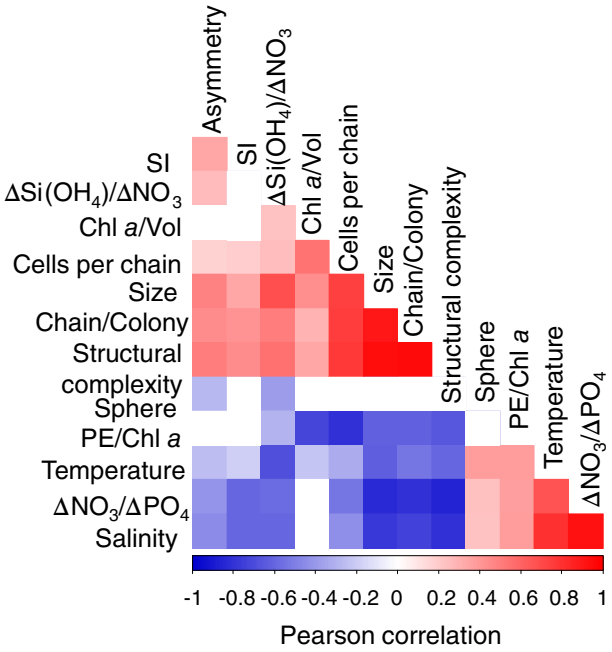

Fig. 6. Correlation plot of environmental factors and the different traits showing statistically significant ($p < 0.05$) positive (red) and negative (blue) correlations. White squares refer to nonstatistically significant relationships. Environmental abbreviations refer to the NO_3 to PO_4 ($\Delta NO_3/\Delta PO_4$) and $Si(OH)_4$ to NO_3 utilization ratios ($\Delta Si(OH)_4/\Delta NO_3$), stratification index (SI) and phycoerythrin to chlorophyll *a* (PE/Chl *a*) and Chl *a* to volume (Chl *a*/Vol) ratios.

both single cells and chains, as well as plastidic ciliates, when compared to Atlantic waters (NWA and NEA). Conversely, Atlantic waters, particularly the NEA, had a higher proportion of small-sized plankton groups, such as picoeukaryotes and *Synechococcus*-like cells. In the NWA, the plankton composition gradually changed between the ARC (45–53°W) and NEA (10–30°W) (Figs. 2a, 4b).

The surface waters of the NWA, which includes the central region of the Labrador Sea and the Irminger Basin, had higher contributions of Arctic waters than the NEA (Yashayaev and Clarke 2008). This explains the gradual increase from west to east in temperature and winter (> 200 m depth) NO_3 concentrations, typically attributed to Atlantic-related waters (Harrison et al. 2013) and the transitional shift in phytoplankton functional groups observed in this study. Moreover, the central deep basin of the Labrador Sea is known to possess highly dynamic hydrography from spring to summer due to the transition from unstratified to thermally stratified waters, which drive variability in species composition (Fragoso et al. 2016, 2017).

The taxonomical composition and relative biovolume of some plankton groups, as derived from the CytoSense analyses (recognized from the images provided), were similar to results from separate microscope (Fragoso et al. 2016, 2018), flow-cytometry (Li and Harrison 2001), and pigment-based studies (Stuart et al. 2000; Fragoso et al. 2017) in the Labrador Sea. For instance, polar or ice-related diatoms have been found to dominate shelf waters of Arctic influence, whereas Atlantic diatoms, such *Ephemera planamembranacea* (Fig. 1c), dominate the central Labrador Sea (Fragoso et al. 2016). The high relative biovolume of diatoms in Arctic waters, decreasing eastward in Atlantic waters, explains the strong drawdown of $Si(OH)_4$ observed (*see* Supporting Information Fig. S5b). The higher concentration of $Si(OH)_4$ relative to NO_3 found in Arctic waters compared to Atlantic waters (Harrison et al. 2013) has also been suggested to shape diatom species composition and the degree of cell wall silicification, with Arctic species having more heavily silicified cells than Atlantic species (Fragoso et al. 2018).

Pulse-shape recording flow cytometry, when compared to other methods, shows good biogeographical agreement for large-sized phytoplankton, such as diatoms (Fragoso et al. 2016, 2017). As expected, taxonomical resolution is limited in terms of nanoflagellates as observed in other studies (Haraguchi et al. 2017). For example, pigment-based community analysis is able to identify chlorophytes as co-dominating Arctic waters using chlorophyll *b* as a biomarker for this group (Fragoso et al. 2017), whereas this group is not distinguishable using the CytoSense parameters. The colonial prymnesiophyte *Phaeocystis pouchetii*, which constitutes an important component of phytoplankton spring blooms in the West Greenland Current (eastern Labrador Sea) (Frajka-Williams and Rhines 2010; Fragoso et al. 2016, 2017), has been previously detected using the CytoSense (Bonato et al. 2015, 2016). In this study, however, *Phaeocystis* colonies were not observed, potentially due to their low abundance in the Labrador Sea during the summer of June 2014 (Fragoso et al. 2016, 2017).

Plastidic aloricate and loricate (tintinnids) ciliates are abundant in Arctic waters (Onda et al. 2017; Kauko et al. 2018; this study) and act as early grazers of the spring plankton community, regulating the size structure by ingesting small flagellates (Pomati et al. 2013) in highly stratified waters (McManus and Fuhrman 1986). In this study, plastidic ciliates may graze on small plankton, which could favor the growth of large diatoms and explain the high percentage of microplankton in Arctic compared to Atlantic waters. Moreover, the plastidic ciliates detected in this study presented internal orange and yellow/green fluorescence, which may relate to their grazing on cryptophytes and/or cyanobacteria (Schoener and McManus 2012), although internal red fluorescence was also observed. The ciliate *M. rubrum* is known to preferentially prey on cryptophytes, ingesting and retaining their chloroplasts for their own use (Gustafson et al. 2000; Myung et al. 2013). Although the plastidic ciliates observed in this study were not *M. rubrum* but lorica-bearing tintinnids (Fig. 1a) and other aloricate ciliates (e.g., *Strombidium* spp.), other studies have suggested that ingestion and retention of cryptophyte chloroplasts is a common feature in many ciliates and certain dinoflagellate taxa (Sjoqvist and Lindholm 2011; Schoener and McManus 2012; Pereira et al. 2017).

In this study, picoeukaryotes were the most abundant phytoplankton group found in Atlantic waters, although they were also present in the other water masses. This group, which includes the prasinophyte *Micromonas pusilla*, has been shown to numerically dominate the entire sub-Arctic North Atlantic (Li et al. 2009; Pettersen et al. 2011; Harrison et al. 2013) and has been assumed as a baseline component that persists throughout the seasons in subpolar waters (Not et al. 2005; Lovejoy et al. 2007). Prokaryotic picophytoplankton includes *Synechococcus*-like cells, being predominantly observed in the NEA. *Synechococcus* abundance has been shown to have a strong link with temperature, having an optimum temperature of 10°C and being rarely detected in subzero waters (Flombaum et al. 2013). Low abundance of cyanobacteria, presumably *Synechococcus*, observed through pigment-based approach has also been observed in cold (< 0°C) Arctic waters of the Labrador Shelf in previous studies in the Labrador Sea (Fragoso et al. 2017). A relationship between *Synechococcus* and warm, saline, and NO_3-rich waters has already been noted in the subpolar NWA, indicating its strong affinity to waters of Atlantic origin (Harrison et al. 2013).

Trait analyses derived from CytoSense

Trait-based approaches have been considered a successful method in ecology because they offer a "common currency" that numerically compares taxa based on their ecological significance (Pomati et al. 2013). To date, the influence of multiple traits in a plankton community has been investigated either using mean community weights from continuous and/or categorical traits (e.g., fuzzy code) (Klais et al. 2017; Rosati et al. 2017; Fragoso et al. 2018) or modeling approaches (Edwards et al. 2013, 2016; Breton et al. 2017). The use of optically derived descriptors adds to the state-of-the-art in trait-based analyses as multiple traits are quantified based on direct observations at the individual cell level, which accounts for variability within plankton groups (Fontana et al. 2016). Trait plasticity within species or taxa are often neglected in trait-based studies, although it has been established as strongly influencing community structure and ecosystem function as much as interspecific variability (Albert et al. 2010; Fontana et al. 2016; Des Roches et al. 2018).

The application of bio-optical descriptors derived from pulse-shape recording automated flow cytometers, including the CytoSense and CytoBuoy, as a way of quantifying plankton traits has been previously applied in natural freshwater communities (Pomati et al. 2013; Fontana et al. 2014, 2016), mesocosms (Pomati and Nizzetto 2013), and laboratory experiments (Takabayashi et al. 2006). These previous studies used the trait descriptors as is, whereas, in this study we used the combination of these descriptors to translate into functional traits typically observed in ecological studies (Table 1). Similar to studies in freshwater systems, functional traits were intrinsically related to their taxonomic grouping in our study (e.g., large diatoms are either large single cells and/or cells living as chains, whereas *Synechococcus* are small and have high ratios of PE/Chl *a*), where cell size is the master trait (Pomati et al. 2013; Fontana et al. 2014, 2016). The positive correlation of cell size with other morphological characteristics in this study highlights that a number of these traits are evolutionarily interrelated (Finkel et al. 2009; Litchman et al. 2010). Functional redundancy of cell size in relation to other morphological traits (asymmetry, coloniality, and structural complexity) can provide further ecological information on a biological community, and may influence ecosystem stability (Peterson et al. 1998) and biodiversity (Nock et al. 2016).

Trait patterns along environmental gradients

While plankton community structure differed between hydrographic regions (ARC, NWA, NEA), traits defined in this study were only statistically different between Arctic and Atlantic waters and not between subregions of the Atlantic (NEA, NWA). A major factor determining these regional difference is due to the traits between water masses being cell size-related, where large and more complex plankton in terms of morphological structure (e.g., diatoms) occur in Arctic waters while small picophytoplankton dominate in Atlantic waters.

In this study, asymmetry, coloniality (e.g., cells per chain), structural complexity, and cell size are common traits found in species assemblages (i.e., diatoms) which correlated negatively with salinity and temperature, meaning that these traits were found in cold, fresh, and more strongly stratified Arctic waters (Fig. 6). Compared to other phytoplankton groups, diatoms are recognized for being large (Le Quéré et al. 2005), often colonial, and exhibiting high structural complexity (i.e., possessing cellular processes, setae, and internal vacuoles) (Fragoso et al. 2018; Tréguer et al. 2018). Diatoms are also known for their high package effect or potential "self-shading" of chloroplasts within the cell (Agustí 1991; Stuart et al. 2000) compared to other (smaller) phytoplankton groups. Strongly illuminated, stratified, ice-melt influenced Arctic waters may select for large cell-sized and colonial diatoms, given that their low optical absorption cross-section protects them from light (including ultraviolet) damage at high intensities (Key et al. 2010).

Highly stratified ice-melt waters, however, may be an unfavorable environment for large diatom chains and colonies, which can sink more readily assuming that they are dense (Margalef 1978). The trade-off for this group may be their highly non-spherical shape (large asymmetry, particularly chains, in addition to their external cellular processes), as observed in this study, which increases drag in the water column, slowing their sinking and maintaining their positive buoyancy (Smetacek 1985; Nguyen et al. 2011). Large diatom cells also possess internal cell vacuoles, often filled with low-density ions (lower than the surrounding seawater), which also allows the cells to maintain a positive or neutral buoyancy (Moore and Villareal 1996; Woods and Villareal 2008; Miklasz and Denny 2010). Large diatom cell size and colony formation are common features of phytoplankton from ice-related waters (Arrigo et al. 2010, 2014; Fragoso et al. 2018; Johnsen et al. 2018).

In Atlantic waters (NEA), traits including spherical shape, high PE/Chl *a* ratios, and high intracellular Chl *a*/Vol ratios may all be attributed to dominance by small phytoplankton, such as picoeukaryotes and *Synechococcus*-like cells. Likewise, the drawdown of NO_3 relative to PO_4 was higher in Atlantic compared to Arctic waters. The sub-Arctic North Atlantic presents a gradual increase in east–west winter NO_3 (> 200 m) (Harrison et al. 2013), suggesting that phytoplankton in surface waters of the NEA were exposed to low NO_3 availability at the time of the study. Small cell size, in addition to high spherical cell shape, is a favorable trait when it comes to low nutrient concentrations because of their inherent high surface area to volume ratio, which promotes rapid nutrient assimilation compared to large cells (Li 2002; Finkel et al. 2009; Marañón 2015). Small cells also have less of a pigment packaging effect than larger cells (i.e., less intracellular shading of the chloroplasts and higher Chl *a* specific absorption; Stuart et al. 2000; Fujiki and Satotu 2002; Johnsen and Sakshaug 2007) so that they are better able to thrive under low light intensities. In this and previous studies (Frajka-Williams et al. 2009; Frajka-Williams and Rhines 2010; Lacour et al. 2015), Atlantic waters were in general less stratified and potentially less well illuminated than Arctic waters, which favors phytoplankton groups that have higher internal concentrations of Chl *a* and accessory pigments per cell (Fragoso et al. 2017).

Photo-physiological traits, such as high PE to Chl *a* ratios observed in *Synechococcus* in Atlantic waters, can also be an advantageous trait given that this accessory pigment provides a chromatic adaptation to clear, open, and highly dynamic (variable in mixing conditions) waters of the Atlantic Ocean. The ubiquitous distribution of *Synechococcus* partly relates to the pigment diversity of its light harvesting antennae and phycobiliproteins (Shukla et al. 2012). Compared to Chl *a*, which absorbs in a narrow band of blue and red light, PE absorbs in a wide part of the spectrum, from blue (460 nm) to yellow (580 nm) (Johnsen and Sakshaug 2007). Thus, the presence of PE in *Synechococcus* is a useful trait as it allows them to adjust for changes in the ambient light color and ultimately maximize photon capture for photosynthesis (Shukla et al. 2012), given that Atlantic waters, in this study, were less stratified (and possibly more dynamic) than Arctic waters.

Conclusions

Here, we have shown that the CytoSense flow cytometer has the capacity to quantify morphological and pigment functional traits based on the optical fingerprints associated with light scattering (forward and sideward) and fluorescence (red, yellow, and orange for Chl *a*, degraded pigments, and phycobiliproteins, respectively) of phytoplankton cells and plastidic ciliates. We used simple output descriptors and translated them into functional traits to demonstrate their variability along an environmental gradient. Functional traits derived from the CytoSense are demonstrated to be a good proxy to explain the segregation of phytoplankton communities, including size spectrum, in contrasting water masses of distinct origin (Arctic vs. Atlantic) in the sub-Arctic North Atlantic Ocean.

Functional traits have previously been used as a common currency to explain the success of certain species in biological communities. This field promises to simplify our interpretation of functionality in biological communities and reduce the information complexity of ecological roles, processes, and interactions, which are fundamental in modeling approaches (Merico et al. 2009). The use of the CytoSense data as a way to quantify traits holds further promise when dealing with plasticity, variability, and dynamics within plankton groups, such as quantifying variability in cell or colony size, which are difficult to quantify via conventional microscopic approaches. Current advances in automated platforms that record in vivo continuous optical measurements, such as the FlowCytoBot (Lambert et al. 2017), CytoSub (Thyssen et al. 2008) and CytoBuoy (Pomati et al. 2011), combined with the trait-based approach used in this study can offer an unique opportunity to study phytoplankton functional trait dynamics at high spatial and temporal scales. Moreover, the use of artificial fluorescence probes to label plankton cellular ultrastructure (e.g., diatom silicification; Leblanc and Hutchins 2005; McNair et al. 2015), as well as gene expression (e.g., fluorescence in situ hybridization; Colin et al. 2017) could be quantified using automated flow cytometers, such as the CytoSense. Such unique approaches can bring forward new opportunities that unravel the linkages between cell biology, evolution, ecosystem structure, and the biogeochemical function of plankton communities.

References

Agustí, S. 1991. Allometric scaling of light absorption and scattering by phytoplankton cells. Can. J. Fish. Aquat. Sci. **48**: 763–767. doi:10.1139/f91-091

Albert, C. H., W. Thuiller, N. G. Yoccoz, R. Douzet, S. Aubert, and S. Lavorel. 2010. A multi-trait approach reveals the structure and the relative importance of intra- vs. interspecific variability in plant traits. Funct. Ecol. **24**: 1192–1201. doi:10.1111/j.1365-2435.2010.01727.x

Arrigo, K. R., T. Mock, and M. P. Lizotte. 2010. Primary producers and sea ice, p. 283–325. *In* D. N. Thomas and G. S. Dieckmann [eds.] Sea ice. Wiley-Blackwell. doi:10.1002/9781444317145.ch8

Arrigo, K. R., Z. W. Brown, and M. M. Mills. 2014. Sea ice algal biomass and physiology in the Amundsen Sea, Antarctica. Elem. Sci. Anthropol. **2**: 28. doi:10.12952/journal.elementa.000028.

Bibby, T. S., Y. Zhang, and M. Chen. 2009. Biogeography of photosynthetic light-harvesting genes in marine phytoplankton. PLoS One **4**: 19–21. doi:10.1371/journal.pone.0004601

Bonato, S., U. Christaki, A. Lefebvre, F. Lizon, M. Thyssen, and L. F. Artigas. 2015. High spatial variability of phytoplankton

assessed by flow cytometry, in a dynamic productive coastal area, in spring: The eastern English Channel. Estuar. Coast. Shelf Sci. **154**: 214–223. doi:10.1016/j.ecss.2014.12.037

Bonato, S., E. Breton, M. Didry, F. Lizon, V. Cornille, E. Lécuyer, U. Christaki, and L. F. Artigas. 2016. Spatio-temporal patterns in phytoplankton assemblages in inshore-offshore gradients using flow cytometry: A case study in the eastern English Channel. J. Mar. Syst. **156**: 76–85. doi:10.1016/j.jmarsys.2015.11.009

Breton, E., U. Christaki, S. Bonato, M. Didry, and L. Artigas. 2017. Functional trait variation and nitrogen use efficiency in temperate coastal phytoplankton. Mar. Ecol. Prog. Ser. **563**: 35–49. doi:10.3354/meps11974

Cermeño, P., C. de Vargas, F. Abrantes, and P. G. Falkowski. 2010. Phytoplankton biogeography and community stability in the ocean. PLoS One **5**: e10037. doi:10.1371/journal.pone.0010037

Clarke, K. R., R. N. Gorley, P. J. Somerfield, and R. M. Warwick. 2014. Change in marine communities: An approach to statistical analysis and interpretation, 3rd ed. PRIMER-E: Plymouth.

Colin, S., L. P. Coelho, S. Sunagawa, C. Bowler, E. Karsenti, P. Bork, R. Pepperkok, and C. de Vargas. 2017. Quantitative 3D-imaging for cell biology and ecology of environmental microbial eukaryotes. Elife **6**: 1–15. doi:10.7554/eLife.26066

Dashkova, V., D. Malashenkov, N. Poulton, I. Vorobjev, and N. S. Barteneva. 2017. Imaging flow cytometry for phytoplankton analysis. Methods **112**: 188–200. doi:10.1016/j.ymeth.2016.05.007

Des Roches, S., D. M. Post, N. E. Turley, J. K. Bailey, A. P. Hendry, M. T. Kinnison, J. A. Schweitzer, and E. P. Palkovacs. 2018. The ecological importance of intraspecific variation. Nat. Ecol. Evol. **2**: 57–64. doi:10.1038/s41559-017-0402-5

Dubelaar, G. B. J., and P. L. Gerritzen. 2000. CytoBuoy: A step forward towards using flow cytometry in operational oceanography. Sci. Mar. **64**: 255–265. doi:10.3989/scimar.2000.64n2255

Dubelaar, G. B. J., P. J. F. Geerders, and R. R. Jonker. 2004. High frequency monitoring reveals phytoplankton dynamics. J. Environ. Monit. **6**: 946–952. doi:10.1039/b409350j

Edwards, K. F., E. Litchman, and C. A. Klausmeier. 2013. Functional traits explain phytoplankton community structure and seasonal dynamics in a marine ecosystem. Ecol. Lett. **16**: 56–63. doi:10.1111/ele.12012

Edwards, K. F., M. K. Thomas, C. A. Klausmeier, and E. Litchman. 2016. Phytoplankton growth and the interaction of light and temperature: A synthesis at the species and community level. Limnol. Oceanogr. **61**: 1232–1244. doi:10.1002/lno.10282

Falkowski, P. G. 2004. The evolution of modern eukaryotic phytoplankton. Science **305**: 354–360. doi:10.1126/science.1095964

Finkel, Z. V., J. Beardall, K. J. Flynn, A. Quigg, T. A. V. Rees, and J. A. Raven. 2009. Phytoplankton in a changing world: Cell size and elemental stoichiometry. J. Plankton Res. **32**: 119–137. doi:10.1093/plankt/fbp098

Flombaum, P., and others. 2013. Present and future global distributions of the marine cyanobacteria *Prochlrococcus* and *Synechococcus*. Proc. Natl. Acad. Sci. USA **110**: 9824–9829. doi:10.1073/pnas.1307701110

Follows, M. J., S. Dutkiewicz, S. Grant, and S. W. Chisholm. 2007. Emergent biogeography of microbial communities in a model ocean. Science **315**: 1843–1846. doi:10.1126/science.1138544

Fontana, S., J. Jokela, and F. Pomati. 2014. Opportunities and challenges in deriving phytoplankton diversity measures from individual trait-based data obtained by scanning flow-cytometry. Front. Microbiol. **5**: 1–12. doi:10.3389/fmicb.2014.00324

Fontana, S., O. L. Petchey, and F. Pomati. 2016. Individual-level trait diversity concepts and indices to comprehensively describe community change in multidimensional trait space. Funct. Ecol. **30**: 808–818. doi:10.1111/1365-2435.12551

Fragoso, G. M., and W. O. Smith. 2012. Influence of hydrography on phytoplankton distribution in the Amundsen and Ross Seas, Antarctica. J. Mar. Syst. **89**: 19–29. doi:10.1016/j.jmarsys.2011.07.008

Fragoso, G. M., A. J. Poulton, I. M. Yashayaev, E. J. H. Head, M. C. Stinchcombe, and D. A. Purdie. 2016. Biogeographical patterns and environmental controls of phytoplankton communities from contrasting hydrographical zones of the Labrador Sea. Prog. Oceanogr. **141**: 212–226. doi:10.1016/j.pocean.2015.12.007

Fragoso, G. M., A. J. Poulton, I. M. Yashayaev, E. J. H. Head, and D. A. Purdie. 2017. Spring phytoplankton communities of the Labrador Sea (2005–2014): Pigment signatures, photophysiology and elemental ratios. Biogeosciences **14**: 1235–1259. doi:10.5194/bg-14-1235-2017

Fragoso, G. M., A. J. Poulton, I. M. Yashayaev, E. J. H. Head, G. Johnsen, and D. A. Purdie. 2018. Diatom biogeography from the Labrador Sea revealed through a trait-based approach. Front. Mar. Sci. **5**: 297. doi:10.3389/fmars.2018.00297

Frajka-Williams, E., P. B. Rhines, and C. C. Eriksen. 2009. Physical controls and mesoscale variability in the Labrador Sea spring phytoplankton bloom observed by Seaglider. Deep-Sea Res. Part I Oceanogr. Res. Pap. **56**: 2144–2161. doi:10.1016/j.dsr.2009.07.008

Frajka-Williams, E., and P. B. Rhines. 2010. Physical controls and interannual variability of the Labrador Sea spring phytoplankton bloom in distinct regions. Deep-Sea Res. Part I Oceanogr. Res. Pap. **57**: 541–552. doi:10.1016/j.dsr.2010.01.003

Fujiki, T., and T. Satotu. 2002. Variability in chlorophyll a specific absorption coefficient in marine phytoplankton as a function of cell size and irradiance. J. Plankton Res. **24**: 859–874. doi:10.1093/plankt/24.9.859

Gustafson, D. E., D. K. Stoecker, M. D. Johnson, W. F. Van Heukelem, and K. Sneider. 2000. Cryptophyte algae are

robbed of their organelles by the marine ciliate *Mesodinium rubrum*. Nature **405**: 1049–1052. doi:10.1038/35016570

Haraguchi, L., H. Jakobsen, N. Lundholm, and J. Carstensen. 2017. Monitoring natural phytoplankton communities: A comparison between traditional methods and pulse-shape recording flow cytometry. Aquat. Microb. Ecol. **80**: 77–92. doi:10.3354/ame01842

Harrison, G. W., K. Yngve Børsheim, W. K. W. Li, G. L. Maillet, P. Pepin, E. Sakshaug, M. D. Skogen, and P. A. Yeats. 2013. Phytoplankton production and growth regulation in the Subarctic North Atlantic: A comparative study of the Labrador Sea-Labrador/Newfoundland shelves and Barents/Norwegian/Greenland seas and shelves. Prog. Oceanogr. **114**: 26–45. doi:10.1016/j.pocean.2013.05.003

Head, E. J. H., L. R. Harris, and I. Yashayaev. 2003. Distributions of *Calanus* spp. and other mesozooplankton in the Labrador Sea in relation to hydrography in spring and summer (1995-2000). Prog. Oceanogr. **59**: 1–30. doi:10.1016/S0079-6611(03)00111-3

Johnsen, G., and E. Sakshaug. 2007. Biooptical characteristics of PSII and PSI in 33 species (13 pigment groups) of marine phytoplankton, and the relevance for pulse-amplitude-modulated and fast-repetition-rate fluorometry. J. Phycol. **43**: 1236–1251. doi:10.1111/j.1529-8817.2007.00422.x

Johnsen, G., M. Norli, M. Moline, I. Robbins, C. von Quillfeldt, K. Sørensen, F. Cottier, and J. Berge. 2018. The advective origin of an under-ice spring bloom in the Arctic Ocean using multiple observational platforms. Polar Biol. **41**: 1197–1216. doi:10.1007/s00300-018-2278-5

Kauko, H. M., et al. 2018. Algal colonization of Young Arctic Sea ice in spring. Front. Mar. Sci. **5**: 199. doi:10.3389/fmars.2018.00199

Key, T., A. McCarthy, D. A. Campbell, C. Six, S. Roy, and Z. V. Finkel. 2010. Cell size trade-offs govern light exploitation strategies in marine phytoplankton. Environ. Microbiol. **12**: 95–104. doi:10.1111/j.1462-2920.2009.02046.x

Klais, R., V. Norros, S. Lehtinen, T. Tamminen, and K. Olli. 2017. Community assembly and drivers of phytoplankton functional structure. Funct. Ecol. **31**: 760–767. doi:10.1111/1365-2435.12784

Lacour, L., H. Claustre, L. Prieur, and F. D'Ortenzio. 2015. Phytoplankton biomass cycles in the North Atlantic subpolar gyre: A similar mechanism for two different blooms in the Labrador Sea. Geophys. Res. Lett. **42**: 5403–5410. doi:10.1002/2015GL064540

Lambert, B. S., R. J. Olson, and H. M. Sosik. 2017. A fluorescence-activated cell sorting subsystem for the imaging flowcytobot. Limnol. Oceanogr.: Methods **15**: 94–102. doi:10.1002/lom3.10145

Le Quéré, C., and others. 2005. Ecosystem dynamics based on plankton functional types for global ocean biogeochemistry models. Glob. Chang. Biol. **11**: 2016–2040. doi:10.1111/j.1365-2486.2005.01004.x

Leblanc, K., and D. A. Hutchins. 2005. New applications of a biogenic silica deposition fluorophore in the study of oceanic diatoms. Limnol. Oceanogr.: Methods **3**: 462–476. doi:10.4319/lom.2005.3.462

Lepesteur, M., J. M. Martin, and A. Fleury. 1993. A comparative study of different preservation methods for phytoplankton cell analysis by flow cytometry. Mar. Ecol. Prog. Ser. **93**: 55–63. doi:10.3354/meps093055

Li, W. K. W. 2002. Macroecological patterns of phytoplankton in the northwestern North Atlantic Ocean. Nature **419**: 154–157. doi:10.1038/nature00983.1

Li, W. K. W., and W. G. Harrison. 2001. Chlorophyll, bacteria and picophytoplankton in ecological provinces of the North Atlantic. Deep-Sea Res. Part II Top. Stud. Oceanogr. **48**: 2271–2293. doi:10.1016/S0967-0645(00)00180-6

Li, W. K. W., F. A. McLaughlin, C. Lovejoy, and E. C. Carmack. 2009. Smallest algae thrive as the Arctic Ocean freshens. Science **326**: 539. doi:10.1126/science.1179798

Litchman, E., C. A. Klausmeier, O. M. Schofield, and P. G. Falkowski. 2007. The role of functional traits and trade-offs in structuring phytoplankton communities: Scaling from cellular to ecosystem level. Ecol. Lett. **10**: 1170–1181. doi:10.1111/j.1461-0248.2007.01117.x

Litchman, E., P. de Tezanos Pinto, C. A. Klausmeier, M. K. Thomas, and K. Yoshiyama. 2010. Linking traits to species diversity and community structure in phytoplankton. Hydrobiologia **653**: 15–28. doi:10.1007/s10750-010-0341-5

Longhurst, A., S. Sathyendranath, T. Platt, and C. Caverhill. 1995. An estimate of global primary production in the ocean from satellite radiometer data. J. Plankton Res. **17**: 1245–1271. doi:10.1093/plankt/17.6.1245

Lovejoy, C., and others. 2007. Distribution, phylogeny, and growth of cold-adapted picoprasinophytes in Arctic Seas. J. Phycol. **43**: 78–89. doi:10.1111/j.1529-8817.2006.00310.x

Malkassian, A., D. Nerini, M. A. van Dijk, M. Thyssen, C. Mante, and G. Gregori. 2011. Functional analysis and classification of phytoplankton based on data from an automated flow cytometer. Cytometry A **79**: 263–275. doi:10.1002/cyto.a.21035

Marañón, E. 2015. Cell size as a key determinant of phytoplankton metabolism and community structure. Ann. Rev. Mar. Sci. **7**: 241–264. doi:10.1146/annurev-marine-010814-015955

Margalef, R. 1978. Life-forms of phytoplankton as survival alternatives in an unstable environment. Oceanol. Acta **1**: 493–509. doi:10.1007/BF00202661

Marie, D., N. Simon, and D. Vaulot. 2005. Phytoplankton cell counting by flow cytometry, p. 253–268. *In* R. A. Anderson [ed.], Algal culturing techniques. Elsevier Academic Press.

Marrec, P., et al. 2018. Coupling physics and biogeochemistry thanks to high-resolution observations of the phytoplankton community structure in the north-western Mediterranean Sea. Biogeosci. **15**: 1579–1606. doi:10.5194/bg-15-1579-2018

McFarland, M., J. Rines, J. Sullivan, and P. Donaghay. 2015. Impact of phytoplankton size and physiology on particulate

optical properties determined with scanning flow cytometry. Mar. Ecol. Prog. Ser. **531**: 43–61. doi:10.3354/meps11325

McGill, B., B. Enquist, E. Weiher, and M. Westoby. 2006. Rebuilding community ecology from functional traits. Trends Ecol. Evol. **21**: 178–185. doi:10.1016/j.tree.2006.02.002

McManus, G. B., and J. A. Fuhrman. 1986. Photosynthetic pigments in the ciliate *Laboea strobila* from Long Island Sound, USA. J. Plankton Res. **8**: 317–327. doi:10.1093/plankt/8.2.317

McNair, H. M., M. A. Brzezinski, and J. W. Krause. 2015. Quantifying diatom silicification with the fluorescent dye, PDMPO. Limnol. Oceanogr.: Methods **13**: 587–599. doi:10.1002/lom3.10049

Menden-Deuer, S., E. Lessard, and J. Satterberg. 2001. Effect of preservation on dinoflagellate and diatom cell volume, and consequences for carbon biomass predictions. Mar. Ecol. Prog. Ser. **222**: 41–50. doi:10.3354/meps222041

Merico, A., J. Bruggeman, and K. Wirtz. 2009. A trait-based approach for downscaling complexity in plankton ecosystem models. Ecol. Model. **220**: 3001–3010. doi:10.1016/j.ecolmodel.2009.05.005

Miklasz, K. A., and M. W. Denny. 2010. Diatom sinkings speeds: Improved predictions and insight from a modified stokes' law. Limnol. Oceanogr. **55**: 2513–2525. doi:10.4319/lo.2010.55.6.2513

Moore, J. K., and T. A. Villareal. 1996. Size-ascent rate relationships in positively buoyant marine diatoms. Limnol. Oceanogr. **41**: 1514–1520. doi:10.4319/lo.1996.41.7.1514

Myung, G., H. S. Kim, J. W. Park, J. S. Park, and W. Yih. 2013. Sequestered plastids in *Mesodinium rubrum* are functionally active up to 80 days of phototrophic growth without cryptomonad prey. Harmful Algae **27**: 82–87. doi:10.1016/j.hal.2013.05.001

Nguyen, H., L. Karp-Boss, P. A. Jumars, and L. Fauci. 2011. Hydrodynamic effects of spines: A different spin. Limnol. Oceanogr.: Fluids Environ. **1**: 110–119. doi:10.1215/21573698-1303444

Nock, C. A., R. J. Vogt, and B. E. Beisner. 2016. Functional traits. In eLS [Ed.] John Wiley & Sons, Ltd.: 1–8. doi:10.1002/9780470015902.a0026282

Not, F., and others. 2005. Late summer community composition and abundance of photosynthetic picoeukaryotes in Norwegian and Barents Seas. Limnol. Oceanogr. **50**: 1677–1686. doi:10.4319/lo.2005.50.5.1677

Onda, D. F. L., E. Medrinal, A. M. Comeau, M. Thaler, M. Babin, and C. Lovejoy. 2017. Seasonal and interannual changes in ciliate and dinoflagellate species assemblages in the Arctic Ocean (Amundsen Gulf, Beaufort Sea, Canada). Front. Mar. Sci. **4**: 16. doi:10.3389/fmars.2017.00016

Pereira, G. C., A. R. Figueiredo, and N. F. F. Ebecken. 2017. Using in situ flow cytometry images of ciliates and dinoflagellates for aquatic system monitoring. Braz. J. Biol. **78**: 240–247. doi:10.1590/1519-6984.05016

Peterson, G., C. R. Allen, G. Peterson, C. R. Allen, and C. S. Holling. 1998. Ecological resilience, biodiversity, and scale. Ecosystems **1**: 6–18. doi:10.1007/s100219900002

Pettersen, R., G. Johnsen, J. Berge, and E. K. Hovland. 2011. Phytoplankton chemotaxonomy in waters around the Svalbard archipelago reveals high amounts of Chl *b* and presence of gyroxanthin-diester. Polar Biol. **34**: 627–635. doi:10.1007/s00300-010-0917-6

Pomati, F., J. Jokela, M. Simona, M. Veronesi, and B. W. Ibelings. 2011. An automated platform for phytoplankton ecology and aquatic ecosystem monitoring. Environ. Sci. Technol. **45**: 9658–9665. doi:10.1021/es201934n

Pomati, F., N. J. B. Kraft, T. Posch, B. Eugster, J. Jokela, and B. W. Ibelings. 2013. Individual cell based traits obtained by scanning flow-cytometry show selection by biotic and abiotic environmental factors during a phytoplankton spring bloom. PLoS One **8**: e71677. doi:10.1371/journal.pone.0071677

Pomati, F., and L. Nizzetto. 2013. Assessing triclosan-induced ecological and trans-generational effects in natural phytoplankton communities: A trait-based field method. Ecotoxicology **22**: 779–794. doi:10.1007/s10646-013-1068-7

Poulton, A. J., and others. 2016. Production of dissolved organic carbon by Arctic plankton communities: Responses to elevated carbon dioxide and the availability of light and nutrients. Deep-Sea Res. Part II Top. Stud. Oceanogr. **127**: 60–74. doi:10.1016/j.dsr2.2016.01.002

Qiu, D., L. Huang, and S. Lin. 2016. Cryptophyte farming by symbiotic ciliate host detected in situ. Proc. Natl. Acad. Sci. USA **113**: 12208–12213. doi:10.1073/pnas.1612483113

Rosati, I., and others. 2017. A thesaurus for phytoplankton trait-based approaches: Development and applicability. Ecol. Inform. **42**: 129–138. doi:10.1016/j.ecoinf.2017.10.014

Schoener, D., and G. McManus. 2012. Plastid retention, use, and replacement in a kleptoplastidic ciliate. Aquat. Microb. Ecol. **67**: 177–187. doi:10.3354/ame01601

Shukla, A., and others. 2012. Phycoerythrin-specific bilin lyase-isomerase controls blue-green chromatic acclimation in marine Synechococcus. Proc. Natl. Acad. Sci. USA **109**: 20136–20141. doi:10.1073/pnas.1211777109

Sieracki, C. K., M. E. Sieracki, and C. S. Yentsch. 1998. An imaging analysis system for automated analysis for marine microplankton. Mar. Ecol. Prog. Ser. **168**: 285–296. doi:10.3354/meps168285

Sjoqvist, C. O., and T. J. Lindholm. 2011. Natural co-occurrence of *Dinophysis acuminata* (Dinoflagellata) and *Mesodinium rubrum* (Ciliophora) in thin layers in a coastal inlet. J. Eukaryot. Microbiol. **58**: 365–372. doi:10.1111/j.1550-7408.2011.00559.x

Smetacek, V. S. 1985. Role of sinking in diatom life-hystory: Ecological, evolutionary and geological significance. Mar. Biol. **84**: 239–251. doi:10.1007/BF00392493

Sosik, H. M., and R. J. Olson. 2007. Automated taxonomic classification of phyoplankton sampled with imaging-in-

flow-cytometry. Limnol. Oceanogr.: Methods **5**: 204–216. doi:10.4319/lom.2007.5.204.

Stuart, V., S. Sathyendranath, E. J. H. Head, T. Platt, B. Irwin, and H. Maass. 2000. Bio-optical characteristics of diatom and prymnesiophyte populations in the Labrador Sea. Mar. Ecol. Prog. Ser. **201**: 91–106. doi:10.3354/meps201091

Takabayashi, M., K. Lew, A. Johnson, A. Marchi, R. Dugdale, and F. P. Wilkerson. 2006. The effect of nutrient availability and temperature on chain length of the diatom, *Skeletonema costatum*. J. Plankton Res. **28**: 831–840. doi:10.1093/plankt/fbl018

Thoisen, C., B. W. Hansen, and S. L. Nielsen. 2017. A simple and fast method for extraction and quantification of cryptophyte phycoerythrin. MethodsX **4**: 209–213. doi:10.1016/j.mex.2017.06.002

Thomas, M. K., S. Fontana, M. Reyes, and F. Pomati. 2018. Quantifying cell densities and biovolumes of phytoplankton communities and functional groups using scanning flow cytometry, machine learning and unsupervised clustering. PLoS One **13**: e0196225. doi:10.1371/journal.pone.0196225

Thyssen, M., G. A. Tarran, M. V. Zubkov, R. J. Holland, G. Grégori, P. H. Burkill, and M. Denis. 2008. The emergence of automated high-frequency flow cytometry: Revealing temporal and spatial phytoplankton variability. J. Plankton Res. **30**: 333–343. doi:10.1093/plankt/fbn005

Thyssen, M., S. Alvain, A. Lefèbvre, D. Dessailly, M. Rijkeboer, N. Guiselin, V. Creach, and L.-F. Artigas. 2015. High-resolution analysis of a North Sea phytoplankton community structure based on in situ flow cytometry observations and potential implication for remote sensing. Biogeosciences **12**: 4051–4066. doi:10.5194/bg-12-4051-2015

Thyssen, M., and others. 2014. Onset of the spring bloom in the northwestern Mediterranean Sea: Influence of environmental pulse events on the in situ hourly-scale dynamics of the phytoplankton community structure. Front. Microbiol. **5**: 1–16. doi:10.3389/fmicb.2014.00387

Tréguer, P., et al. 2018. Influence of diatom diversity on the ocean biological carbon pump. Nat. Geosci. **11**: 27–37. doi:10.1038/s41561-017-0028-x

Vaulot, D., C. Courties, and F. Partensky. 1989. A simple method to preserve oceanic phytoplankton for flow cytometric analyses. Cytometry **10**: 629–635. doi:10.1002/cyto.990100519

Welschmeyer, N. A. 1994. Fluorometric analysis of chlorophyll a in the presence of chlorophyll b and pheopigments. Limnol. Oceanogr. **39**: 1985–1992. doi:10.4319/lo.1994.39.8.1985

Woods, S., and T. A. Villareal. 2008. Intracellular ion concentrations and cell sap density in positively buoyant oceanic phytoplankton. Nova Hedwigia **133**: 131–145.

Yashayaev, I., and A. Clarke. 2008. Evolution of North Atlantic water masses inferred from Labrador Sea salinity series. Oceanography **21**: 30–45. doi:10.5670/oceanog.2008.65

Acknowledgments

We would like to thank Brian King, Mark C. Stinchcombe, and Sinhue Torres-Valdes (National Oceanography Centre) for sharing the nutrient and hydrographic data from JR302 cruise. Thanks to the officers and crew of the RSS James Clark Ross. G. M. F. was funded by a Brazilian Ph.D. studentship, Science without Borders (CNPq, 201449/2012-9). This research was also partially funded by UK Ocean Acidification, a Natural Environment Research Council grant (NE/H017097/1) through an added value award to A. J. P. Contributions from G. J. are from the Center of Excellence for Autonomous Marine Operations and Systems (AMOS) at NTNU (Norwegian Research Council, Project 223254).

Conflict of Interest

None declared.

Submitted 25 July 2018
Revised 10 January 2019
Accepted 12 April 2019

Associate editor: Heidi Sosik